SCIENTIFIC REP🟥RTS

Plasmonic silver quantum dots coupled with hierarchical TiO$_2$ nanotube arrays photoelectrodes for efficient visible-light photoelectrocatalytic hydrogen evolution

Zichao Lian[*], Wenchao Wang[*], Shuning Xiao, Xin Li, Yingying Cui, Dieqing Zhang, Guisheng Li & Hexing Li

A plasmonic Ag/TiO$_2$ photocatalytic composite was designed by selecting Ag quantum dots (Ag QDs) to act as a surface plasmon resonance (SPR) photosensitizer for driving the visible-light driven photoelectrocatalytic hydrogen evolution. Vertically oriented hierarchical TiO$_2$ nanotube arrays (H-TiO$_2$-NTAs) with macroporous structure were prepared through a two-step method based on electrochemical anodization. Subsequently, Ag QDs, with tunable size (1.3-21.0 nm), could be uniformly deposited on the H-TiO$_2$ NTAs by current pulsing approach. The unique structure of the as-obtained photoelectrodes greatly improved the photoelectric conversion efficiency. The as-obtained Ag/H-TiO$_2$-NTAs exhibited strong visible-light absorption capability, high photocurrent density, and enhanced photoelectrocatalytic (PEC) activity toward photoelectrocatalytic hydrogen evolution under visible-light irradiation ($\lambda > 420$ nm). The enhancement in the photoelectric conversion efficiency and activity was ascribed to the synergistic effects of silver and the unique hierarchical structures of TiO$_2$ nanotube arrays, strong SPR effect, and anti-shielding effect of ultrafine Ag QDs.

Photoelectrocatalysis (PEC) water splitting is widely recognized as one of the most promising ways to large-scale production of hydrogen in the future[1], and different materials with kinds of structures such as TiO$_2$[2], Fe$_2$O$_3$[3,4] etc. have been designed for PEC. Currently, TiO$_2$ remains a proper choice as an electrode material for PEC, because of its nontoxicity, photostability and low cost. To date, various TiO$_2$ nanostructures, including nanoparticles[5], nanospheres[6], nanorods[7], nanowires[8], and nanotubes[9,10], have been fabricated for their special physicochemical properties. Among the different geometric shapes, the aligned TiO$_2$ nanotube arrays (TiO$_2$-NTAs) obtained by the anodization of Ti sheet have aroused considerable scientific interest[11]. TiO$_2$-NTAs could offer a large internal surface area, thus supplying several reaction active sites. In addition, the aligned nanotube structure allows for the absorption of light by reducing the loss of light reflection, because photons that enter the nanotubes are less likely to escape due to multiple reflections by the walls[12]. Recently, forming hierarchical TiO$_2$ nanotube arrays by coating

Key Laboratory of Resource Chemistry of Ministry of Education, Shanghai Key Laboratory of Rare Earth Functional Materials, College of Life and Environmental Science, Shanghai Normal University, Shanghai, 200234, China (PRC). [*]These authors contributed equally to this work. Correspondence and requests for materials should be addressed to G.S.L. (email: liguisheng@shnu.edu.cn) or D.Q.Z. (email: dqzhang@shnu.edu.cn)
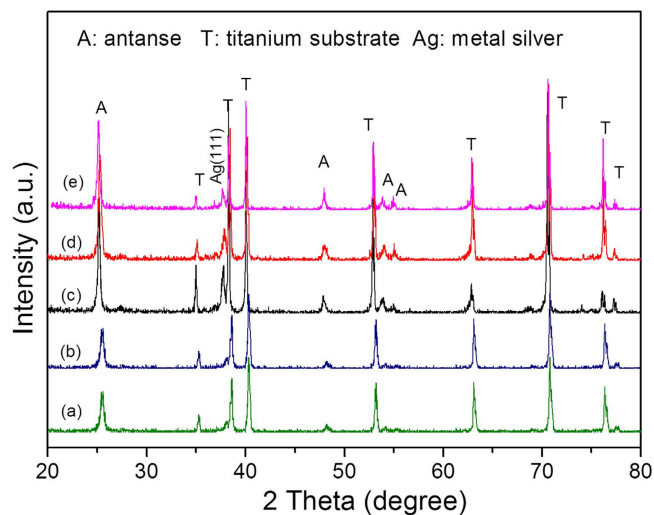
Figure 1. XRD spectra. XRD patterns of (**a**) the as-prepared H-TiO$_2$-NTAs, and Ag/H-TiO$_2$-NTAs with various pulse electro-deposition time of (**b**) 10 s, (**c**) 20 s, (**d**) 50 s, (**e**) 100 s.

a photonic crystal layer with larger pore size has been proved an effective way to enhance the light adsorption capability[13].

However, the practical application of pure TiO$_2$-NTAs is still limited by the broad band gap (3.2 eV for anatase) and fast recombination rate of photo-generated electron-hole pairs. Coupling TiO$_2$-NTAs with noble metals, including Au[14], Ag[15], Cu[16], Pd[17], was utilized to overcome the inherent problem of TiO$_2$ owing to the high conductivity and SPR effect of noble metals. So far, the nanocrystals of noble metals, especially Ag, have been attracting considerable attention. This is because they could strongly interact with light (in visible or infrared region) due to their extraordinary localized SPR properties and their remarkable photostability[18–20]. Nevertheless, coupling TiO$_2$-NTAs with noble metal always suffers from the light shielding effect resulting from the larger nanocrystals size of metal[21]. Thus, it is highly required to obtain ultrafine Ag nanocrystals uniformly coupled TiO$_2$-NTAs, while keeping the excellent SPR effect of silver metal. Small size of Ag nanocrystals could be favorable for decreasing the photo-generated electron transfer distance and accelerating the electron transfer rate, thus the SPR-induced photo-electron transfer efficiency would be greatly enhanced[17]. Furthermore, the Ag nanocrystals were proved to be able to possess strong SPR effect even its size was decreased to below 2 nm[22].

Herein, highly dispersed ultrafine Ag nanocrystals were uniformly loaded on the pore-wall surface of the hierarchical TiO$_2$ nanotube arrays via pulse electro-deposition route[23]. The average size of Ag nanocrystals could be precisely controlled from 1.3 nm to 21.0 nm through carefully controlling the pulse electro-deposition time. Thus, the as-formed ultrafine Ag QDs enhanced hierarchical TiO$_2$-NTAs film was utilized as a working electrode for the photoelectrocatalytic hydrogen evolution under visible-light irradiation, with the aid of a small bias voltage of 0.7 V vs a saturated calomel electrode (SCE). The results indicated that loading Ag nanocrystals could greatly enhance the visible-light driven performance in photoelectrocatalytic hydrogen evolution owing to the strong SPR effect of Ag and free light-shielding. The optimal size of Ag coupled with TiO$_2$ TNAs was about 2.5 nm, delivering for the highest photoelectrocatalytic H$_2$ evolution rate of about 124.4 μmol*cm^{-2}*h^{-1}. Such Ag nanocrystals enhanced hierarchical TiO$_2$-NTAs (Ag/H-TiO$_2$-NTAs) electrode exhibited excellent photoelectrocatalytic activity toward hydrogen evolution under visible-light irradiation ($\lambda > 420$ nm).

Results

Characterizations of Ag/H-TiO$_2$-NTAs composites. In order to identify the crystal phase of H-TiO$_2$-NTAs and Ag/H-TiO$_2$-NTAs, the X-ray diffraction (XRD) measurement was used as the results shown in Fig. 1. For the pure H-TiO$_2$-NTAs, all diffraction peaks could be indexed to the TiO$_2$ anatase phase (JCPDS file no: 21-1272) and the Ti metal phase (JCPDS file no: 44-1294). There were no obvious differences between 10s-Ag/H-TiO$_2$-NTAs and pure H-TiO$_2$-NTAs. No Ag diffraction peaks could be clearly identified, and it may be attributed to the ultrafine size, high dispersity, and low loaded content of Ag nanocrystals. To the case of the 20 s, 50 s, 100 s Ag/H-TiO$_2$-NTAs samples, there were additional diffraction peaks at 2θ values of 37.7 °, which could be attributed to the (111) crystal planes of the cubic Ag phase (JCPDF file no: 65-8428)[24]. It should be noted that the other diffraction peaks ascribed to cubic Ag phase were not clearly distinguished because they were overlapped with those of anatase TiO$_2$ and pure Ti metal. The XRD results indicated that the Ag/TiO$_2$ composite electrodes prepared by the pulse electro-deposition method were composed of Ag nanocrystals and crystalline TiO$_2$ anatase.
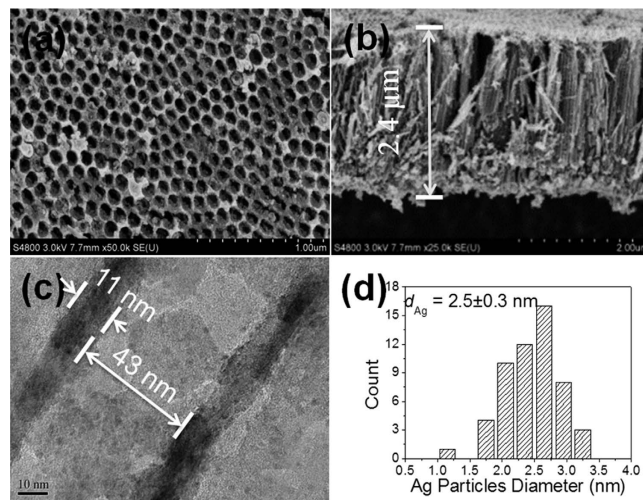
Figure 2. FESEM, TEM images and size distribution. Top view of FESEM image (**a**) cross-section view FESEM image (**b**) of H-TiO$_2$-NTAs, (**c**) TEM image of 20s-Ag/H-TiO$_2$-NTAs, and (**d**) size distribution of Ag QDs located on the pore wall of 20s-Ag/H-TiO$_2$-NTAs.

FESEM, TEM images and size distribution.   Figure 2a presents a top view field emission scanning electron microscope (FESEM) image of the as-prepared H-TiO$_2$-NTAs. A unique top layer with a peri-odically porous structure could be clearly observed. The average diameter of the pores was 70 ± 2.0 nm, and the thickness of the walls was 22 ± 1.0 nm. The thickness of the bottom TiO$_2$-NTA layer was about 2.4 μm, as shown in Fig. 2b. It should be noted that the length of the TiO$_2$-NTAs in this study was rationally chosen, as it has been reported that about 2.0 μm was the maximum penetration depth of the incident light in TiO$_2$-NTAs[13]. Further increasing the tube length would improve its electronic resistance, inhibiting the photo-generated transmission located in the TiO$_2$-NTAs. A cross-section FESEM view of the H-TiO$_2$-NTAs (Fig. 2b) indicated a uniformly non-flat, concave-like top layer, which was closely connected with the bottom TiO$_2$-NTAs. The concaves in the top layer were expected to work as nano-mirrors for light reflection and scattering[13]. From Fig. 2c,d, one could clearly see that silver QDs were uniformly deposited on the surface of the pore wall of H-TiO$_2$-NTAs with an average size about 2.5 nm *via* the proposed pulse electro-deposition route. The crystal lattice of Ag and TiO$_2$ can be clearly seen shown in Fig. S1. The lattice space of lattice facet with Ag (111) was 0.238 nm, and the lattice spacing of 0.352 nm was assigned to the (101) facet of TiO$_2$. Besides, it can also be observed that the inner diameter of the nanotubes was 43 ± 1.0 nm, and the thickness of the TiO$_2$ nanotubes was 11 ± 2.0 nm. Both of the values were much lower than those of the porous surface layer of TiO$_2$. As shown in Fig. S2, the size of the loaded Ag nanocrystals could be tunable from about 1.3 nm to 21.0 nm by increasing the pulse electro-deposition time from 10 s to 100 s. The space of the inner nanotubes were almost totally com-plete occupied by the large Ag nanocrystals upon choosing 100 s electro-deposition time. Such blocking effect resulting from the over growth of Ag nanocrystals will not allow the light to penetrate into the TiO$_2$ nanotubes *via* multiple-reflection as shown in Fig. 3. It was obvious that Ag, as photosensitizer, could exhibit SPR effects when it was irradiated with visible-light (490 nm $> \lambda >$ 390 nm)[19,25]. With the aid of SPR effect, hot electrons were able to transfer from Ag nanocrystals into the conduction band of TiO$_2$-NTAs. Meanwhile, the wall of TiO$_2$ nanotubes possessed excellent ability to transfer electrons, allowing more electrons to be trapped by protons with the formation of H$_2$. Thus, it was reasonable that Ag/H-TiO$_2$-NTAs would exhibit enhanced photoelectrocatalytic activities in H$_2$ evolution owing to the SPR effect and anti-shielding effect of ultrafine Ag QDs.

XPS analysis.   In order to acquire in-depth fundamental information on the interaction of Ag with TiO$_2$, the X-ray photoelectron spectroscopy (XPS) technique was employed to analyze the specific sur-face composition and elemental binding energy of H-TiO$_2$-NTAs and 20 s Ag/H-TiO$_2$-NTAs. Figure 4a exhibited the high-resolution spectrum of Ag 3d from the Ag modified H-TiO$_2$ NTAs sample. The Ag 3d$_{5/2}$ core level of 20 s Ag/H-TiO$_2$-NTAs could be fitted with a single peak at a binding energy of 368.5 eV, which was attributed to the presence metallic Ag^0. A significant positive shift of the binding energy for Ag 3d$_{5/2}$ relative to 368.0 eV of the bulk Ag was identified due to the electron transfer from Ag to oxygen vacancies of the TiO$_2$.[9] Such positive shift may be attributed to the low work function of metal Ag. Moreover, a small negative shift of the Ti 2p$_{3/2}$ after loading Ag (shown in Fig. 4b) also revealed the feasibility of the electron transfer between the Ag and H-TiO$_2$-NTAs.
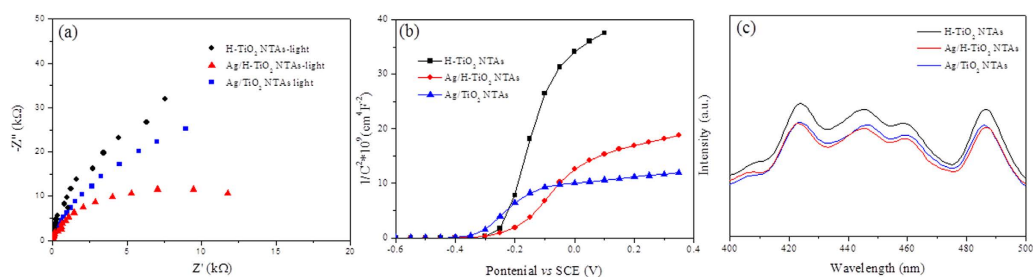
Electrochemical testing and Photoluminescence.   The interfacial properties between the elec-trode and the electrolyte were detected by electrochemical impedances spectroscopy (EIS) measurements.
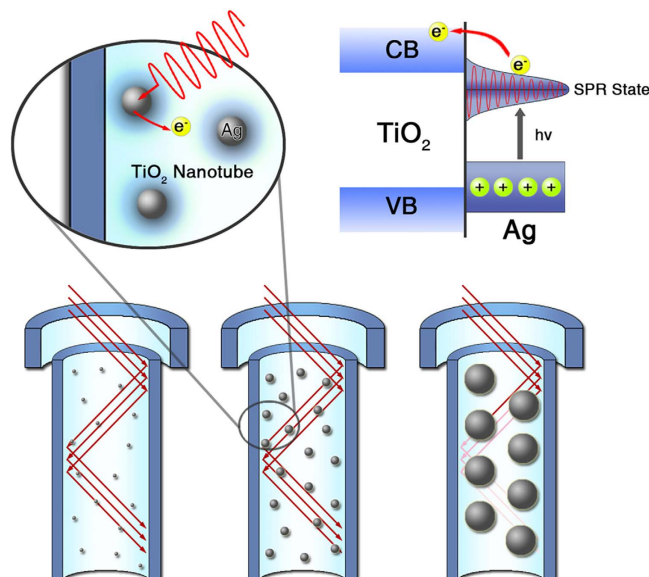
Figure 3. Schematic diagram. The light penetration mechanism in the Ag nanocrytals loaded H-TiO$_2$-NTAs.
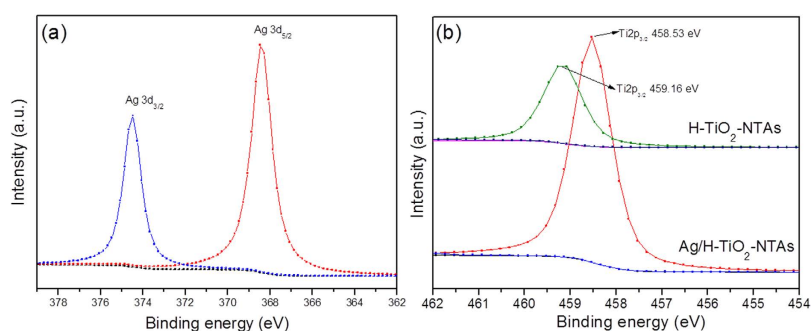
Figure 4. XPS analysis. High resolution XPS of (**a**) Ag 3d of 20s-Ag/H-TiO$_2$-NTAs and (**b**) Ti 2p of H-TiO$_2$-NTAs and 20s-Ag/H-TiO$_2$-NTAs.

Figure 5. Electrochemical testing and Photoluminescence. (**a**) Nyquist plot of electrochemical impedance spectra, (**b**) Mott-Schottky plots, and (**c**) photoluminescence (PL) spectra with the excited wavelength at 280 nm of H-TiO$_2$-NTAs, 20s Ag/H-TiO$_2$-NTAs, and 20s Ag/TiO$_2$-NTAs.

A semicircle in the Nyquist plot at high frequency represented the charge-transfer process, while the diameter of the semicircle reflected the charge-transfer resistance (Fig. 5a). It was clear that the arch for Ag/H-TiO$_2$-NTAs under visible light (>420 nm) illumination was much smaller than that for H-TiO$_2$-NTAs, implying that decoration with Ag QDs could significantly enhance the electron mobility by reducing the recombination of electron-hole pairs. *Via* comparison of the different samples, the arch value for Ag/TiO$_2$-NTAs without porous top layer was in the middle among them under visible-light irradiation. It was noted that Ag QDs exhibited an important role in the solution-action process of

electron transfer. In addition, the capacitance measurement was performed on the electrode/electrolyte according to the Mott-Schottky equation[26],

$$\frac{1}{C^2} = \frac{2}{N_D e \varepsilon_0 \varepsilon}\left(E - E_{FB} - \frac{kT}{e}\right)$$

(1)

where C is the space charge capacitance in the semiconductor, N_D is the electron carrier density, e is the elemental charge value, ε_0 is the permittivity of the vacuum, ε is the relative permittivity of the semiconductor, E is the applied potential, E_{FB} is the flat band potential, T is temperature, and k is the Boltzmann constant. Figure 5b displays the Mott-Schottky plots of $1/C^2$ as a function of the applied potential, from which the positive slopes (i.e., lines) were observed, suggesting n-type semiconductors. Furthermore, the plots were extrapolated to $1/C^2 = 0$ to estimate the values of E_{FB} at -0.251 V and -0.213 V for H-TiO$_2$ NTAs and Ag/H-TiO$_2$-NTAs, respectively. A 38 mV increase of E_{FB} implied steeper band bending, forming strong Schottky junction between TiO$_2$ and Ag, and thereby facilitating the electron transfer. In addition, the carrier density N_D could also be calculated from Fig. 3b by using the following equation[13]:

$$N_D = \frac{2}{e \varepsilon_0 \varepsilon}\left(\frac{dE}{d\left(\frac{1}{C^2}\right)}\right)$$

(2)

As $e = 1.6 \times 10^{-19}$ C, $\varepsilon_0 = 8.86 \times 10^{-12}$ F/m, and $\varepsilon = 48$ for anatase TiO$_2$, the N_D values of H-TiO$_2$-NTAs and Ag/H-TiO$_2$-NTAs are determined as 1.42×10^{17} cm^{-3} and 4.32×10^{17} cm^{-3}, respectively. Consequently, the higher N_D of Ag/ H-TiO$_2$-NTAs would result in lower resistance and faster charge transfer rate, leading to enhanced PEC performance.

We noted that the capability of charge separation by Ag QDs could also be verified by the analysis of the photoluminescence (PL) spectra as shown in Fig. 3c. PL measurements were often employed to study surface processes involving electron-hole recombination of TiO$_2$. Briefly, after irradiation of the photocatalysts, electron-hole pairs underwent a recombination process, and photons were then emitted, resulting in PL[18]. As shown in Fig. 5c, the peak at 424 nm (corresponding to 2.92 eV) could be attributed to self-trapped excitations located on the TiO$_2$ octahedral. The peaks at 446 nm, 459 nm, and 487 nm (corresponding to 2.78 eV, 2.70 eV, and 2.55 eV, respectively) were also observed, which were associated with the oxygen vacancies[27–30]. The PL intensity for 20 s Ag/H-TiO$_2$-NTAs was much lower than that of H-TiO$_2$-NTAs, indicating a reduced charge carrier recombination resulting from the formation of Schottky junction between TiO$_2$ and Ag nanocrystals[31]. It was also noted that the pure H-TiO$_2$-NTAs exhibited a lower intensity of PL compared to that of the Ag loaded traditional TiO$_2$ nanotube arrays (20 s Ag/TiO$_2$-NTAs). This suggested that the formation of hierarchical structured TiO$_2$ nanotubes played an important role for inhibiting the electron-hole recombination.
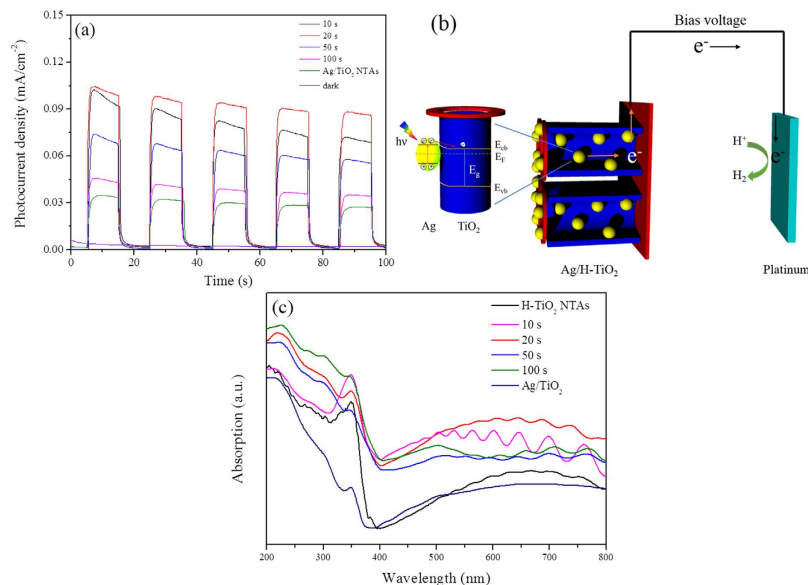
Discussion

Photoelectrochemical properties of the pure and Ag QDs modified H-TiO$_2$-NTAs and schematic diagram of SPR charge carrier transfer mechanisms.   To evaluate the enhanced PEC performance of the fabricated Ag/H-TiO$_2$-NTAs under visible-light irradiation, the transient photocurrent was done to verify the separation of photo-induced charges. Chronoamperometric I-t curves were measured and recorded in Fig. 6a by irradiating the electrodes with visible-light ($\lambda > 420$ nm) at a potential of 0.7 V vs SCE. It was surprising that 20 s-Ag/H-TiO$_2$-NTAs with hierarchical structures exhibited a very high photocurrent density (0.104 mA/cm^{-2}), about 3 times of that (0.034 mA/cm^{-2}) of the traditional Ag/TiO$_2$-NTAs. Such greatly enhanced photo-response ability could be attributed to its special structure and enhanced SPR intensity. It was also noted that the photocurrent density of Ag/H-TiO$_2$-NTAs increased with the pulse deposited time of Ag nanocrystals. Prolonging the deposition time over 20 s could result in the decrease of photocurrent density because of the formation larger size of Ag nanocrystals, which could shield the multi-reflection of light in the hierarchical TiO$_2$-NTAs.

As schematically presented in Fig. 6b, Ag QDs, as the sensitizer, were excited under visible-light irradiation. Hot electrons from the SPR of metal Ag, possessed enough energy to overcome the Schottky barrier between the Ag and TiO$_2$-NTAs[32,33] and inject into the conduction band of the adjacent H-TiO$_2$-NTAs. Meanwhile, these hot electrons would transfer along the wall of TiO$_2$-NTAs, which could provide the fast transfer paths. Besides, the ultrafine size of Ag nanocrystals could also be favorable for enhancing the transfer rate of electrons owing to its short electron-migration distance between excited Ag and the wall of TiO$_2$-NTAs.

With the aid of external bias voltage, the electrons could transfer from photoanode to cathode (platinum foil), and further react with the H$^+$ ions to form H$_2$ on the surface of Pt foil. The positive charges formed on Ag QDs possessed certain oxidation ability to participate in oxidation reaction, in which ethylene glycol was transfered to glyoxal, oxalic acid or other by-products. In addition, the optical properties of H-TiO$_2$-NTAs and Ag/H-TiO$_2$-NTAs samples were investigated by UV-vis diffuse reflectance spectroscopy (DRS). As shown in Fig. 6c, the absorption edge at a wavelength lower than 380 nm could be attributed to the intrinsic band-gap absorption of anatase TiO$_2$. The absorption of bare H-TiO$_2$-NTAs

Figure 6. Photoelectrochemical properties of the pure and Ag QDs modified H-TiO$_2$-NTAs and schematic diagram of SPR charge carrier transfer mechanisms. (**a**) Photocurrent responses in the light on-off process (0.7 V vs. SCE): under illumination of visible light with wavelength >420 nm with 20 s light on/off cycles. (**b**) SPR charge carrier transfer under visible light irradiation at Ag/H-TiO$_2$ interface and the PEC process for H$_2$ evolution. (**c**) DRS of H-TiO$_2$-NTAs, Ag/TiO$_2$ and Ag/H-TiO$_2$-NTAs with different deposition time: 10 s, 20 s, 50 s, 100 s.
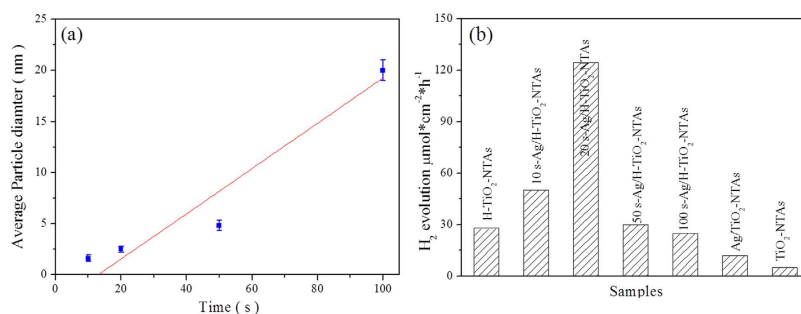
Figure 7. Size of Ag QDs and photocatalytic H$_2$ production. (**a**) The size of Ag quantum dots *via* the pulse electron-deposition time; (**b**) the hydrogen evolution rate by using various samples as photoanodes and Pt foil as cathodes, at 0.7 vs. SCE in a PEC cell containing a 2 M ethylene glycol and 0.5 M Na$_2$SO$_4$ solution under 300 W Xe lamp (>420 nm filter) irradiation.

(Fig. 6c) in the visible-light region could be assigned to the hierarchical ordered nanoarrays. Such ordered TiO$_2$ nanoarrays can form the photonic crystals, allowing the TiO$_2$ films to adsorb visible-light[13]. However, such adsorbed visible light cannot be utilized to activate the pure TiO$_2$ for the formation of electro-hole pairs. Upon loading Ag nanocrystals, Ag/H-TiO$_2$-NTAs exhibited similar multi-peaks in the visible-region and a significant enhancement of visible-light absorption due to the SPR absorption of the Ag QDs. Among all these Ag enhanced H-TiO$_2$-NTAs samples, 20s Ag/H-TiO$_2$-NTAs displayed the highest SPR intensity, indicating that the SPR effect of Ag was well maintained even its size was decreased to about 2.5 nm *via* carefully choosing the pulse electro-deposition route. This was consistent with the measured SPR wavelength of 440 nm of the same-sized Ag[22] nanocrystals dispersed in solution. And an enhanced visible-light absorption region (wavelength 400-550 nm) was obvious when the Ag NPs size was very small[34] compared with other samples (in Fig. S2). It should be pointed out that further increasing the size of Ag nanocrystals, *via* extending the pulse electron-deposition time over 20 s, resulted in a decrease of the SPR intensity in Fig. 6c. Such decrease could be ascribed to the light shielding effect of the Ag nanocrystals with larger grain size on the pore wall of TiO$_2$ nanotubes.

Size of Ag QDs and photocatalytic H$_2$ production. As shown in Fig. 7a, the size of Ag QDs could be tuned from 1.6 ± 0.3 nm to 20 ± 1.0 nm *via* choosing various pulse-deposition time. Based on the

linear fitting equation ($y = -2.9 + 0.22x$, y represents the size of Ag QDs, x is the deposition time), it was noted that the size of Ag QDs could be controlled by the deposition time consistent with a linear variation. Thus, the pulse deposition method was a suitable route for the fabrication of Ag QDs with controllable size. These results were consistent with the SEM images in Fig. S2. Figure 7b shows the hydrogen generation performance of Ag QDs enhanced hierarchical TiO_2 nanotubes arrays *via* choosing traditional TiO_2 nanotubes as standard. The sample of 20 s Ag/H-TiO_2-NTAs exhibited the highest H_2 evolution rate ($124.5 \mu mol^*cm^{-2*}h^{-1}$) among all these Ag QDs modified hierarchical TiO_2 nanotube arrays. Also it indicated that the macroporous structure covering on the surface of TiO_2 nanotubes contributed lots to enhancing the photoelectrocatalytic activity of electrodes compared to the traditional TiO_2 nanotubes. The amount of hydrogen production exhibited a volcanic pattern from H-TiO_2-NTAs to the Ag/H-TiO_2-NTAs with increasing the size of Ag QDs (1.3 nm to 21.0 nm). The relative low H_2 production rate over 10 s-Ag/H-TiO_2-NTAs was attributed to the lower loaded amount of Ag. The poor H_2 production rate over H-TiO_2-NTAs with large size of Ag QDs may be attributed to the shielding effect toward light of the sizes, which was consistent with the order of light absorption capability in visible-light region as shown in Fig. 6c. It should be pointed out that the H_2 evolution rate of hierarchical TiO_2-NTAs, upon being loaded Ag QDs (20 s deposition time), exhibited a significant increase, more than 3.45 times of that of pure hierarchical TiO_2-NTAs. However, the H_2 production rate of Ag/TiO_2-NTAs only exhibited an increase about 1.4 times compared to that of pure TiO_2-NTAs. These results could further confirm that the hierarchical structure with modification of Ag QDs would enhance the photoelectrocatalytic activity for H_2 production. It might be attributed to the strong Ag-TiO_2 interaction and the excellent light-utilization efficiency of Ag QDs and H-TiO_2-NTAs.

In summary, Ag QDs enhanced hierarchical TiO_2-NTAs electrode was fabricated for effectively driving H_2 evolution through photoelectrocatalytic water-splitting under visible-light ($\lambda > 420$ nm) irradiation. Ag QDs with various average size (1.3-21.0 nm) could be uniformly deposited on the surface of the TiO_2 hierarchical nanotubes. Owing to the strong SPR effect and anti-shielding effect of ultrafine Ag QDs, and the unique property of hierarchical structures of TiO_2 nanotube arrays, the photoelectric conversion efficiency and activity were greatly increased. Especially, the special hierarchical TiO_2 nanotubes with macroporous layers was proved effective for enhancing the interaction between Ag QDs and TiO_2, with the formation of high H_2 evolution activity.

Methods

Materials. Titanium sheets (0.3 mm thick, 99.5%) were purchased from Shanghai Right Titanium Industry Co., Ltd. ethylene glycol (EG), ammonium fluoride, silver nitrate, sodium nitrate, sodium sulfate, acetone and ethanol of analytical grade were obtained from Aladdin Company without further purification. All solutions were prepared using deionized (DI) water with a resistivity of 18.2 MΩ cm prepared by Millipore system.

Preparation of H-NTAs. A pure TiO_2 nanotube arrays electrode was fabricated by an electrochemical anodic oxidation technique. Prior to anodization, the titanium sheets were rinsed in an ultrasonic bath of acetone, ethanol and distilled water for 15 min successively. The anodization was carried out using a conventional two-electrode system with the Ti sheet as the working electrode and a Pt foil (99.99%, 0.1 mm, 2 cm * 2 cm) as the counter electrode, respectively. All electrolytes consisted of 0.5 wt% NH_4F in ethylene glycol solution and 2 vol% water. Firstly, the Ti sheet was anodized at 60 V for 1.5 h, then the anodized Ti sheet was ultrasonically removed in DI water. Subsequently, a second anodization of the same Ti sheet was performed at 30 V for 0.5 h. All the anodization processes were carried out at 30 °C. After the two-step anodization, the prepared hierarchical structure TiO_2-NTAs samples were cleaned with DI water. All the as-anodized samples were crystallized by ambient annealing (500 °C) with a heating and cooling rate of 2 °C min^{-1} for 2 h.

Preparation of Ag/H-NTAs. A two-electrode setup was used for pulse electrodeposition by using a H-TiO_2-NTAs electrode as the working electrode, Pt sheet as the counter electrode, 1 mM $AgNO_3$ and 10 mM $NaNO_3$ as electrolyte solution. For Ag deposition, a current pulsing approach was utilized *via* choosing a cathodic pulse (-25 mA 0.1 s) and a relation time (0 mA, 0.3 s) in 1 mM $AgNO_3$ as well as 10 mM $NaNO_3$ at room temperature with magnetic string at 200 rpm and different deposited time. The as-obtained products of Ag QDs modified H-TiO_2 were labeled as t-Ag/H-TiO_2-NTAs, t represents the time of depositing Ag QDs. All the procedures were showed in Fig. 8. As a reference, the Ag/TiO_2-NTAs were prepared using an one-step anodization route (30 V, 0.5 h and 30 °C), and followed by the pulse electrodeposition (deposition time: 20 s) with the same method in the preparation of Ag/H-TiO_2-NTAs as shown in Fig. S3.

Materials characterizations. X-ray diffraction (XRD) patterns were collected on a Rigacu Dmax-3C with Cu Kα radiation. Selected area electron diffraction (SAED) images and transmission electronic microscopy (TEM) morphologies were recorded on a JEM-2010 instrument. Field emission scanning electron microscopy (FESEM) images were performed on a JEOL JSM-6380LV. The photoluminescence (PL) spectra were recorded on a Varian Cary-Eclipse 500 Raman spectra, and UV-vis diffuse reflectance spectra (UV-vis DRS) were conducted on Dilor Super LabRam II and MC-2530 instruments, respectively.
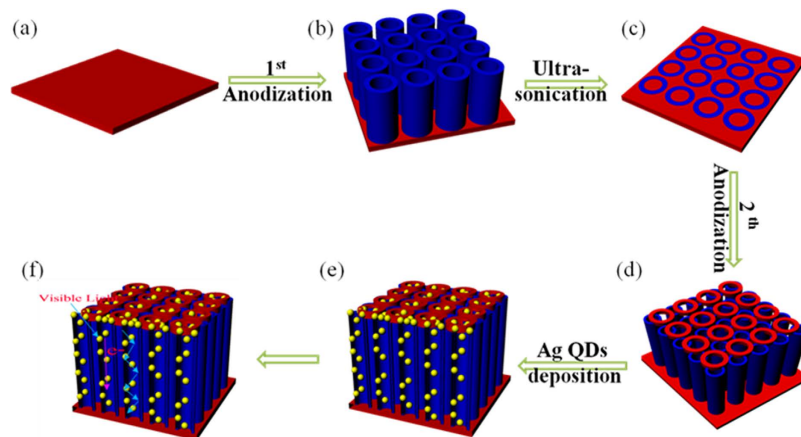
Figure 8. Schematic diagram of the Ag/H-TiO₂-NTAs fabrication procedure. (**a**) Ti foil, (**b**) first anodized TiO₂ nanotubes, (**c**) nanoprints left on the Ti foil, (**d**) Second anodized on the TiO₂ NTAs, (**e**) Ag QDs deposition on the H-TiO₂-NTAs *via* a pluses deposition, (**f**) Top larger pore enhancing SPR of Ag QDs and multiple reflections in the H-TiO₂-NTAs.
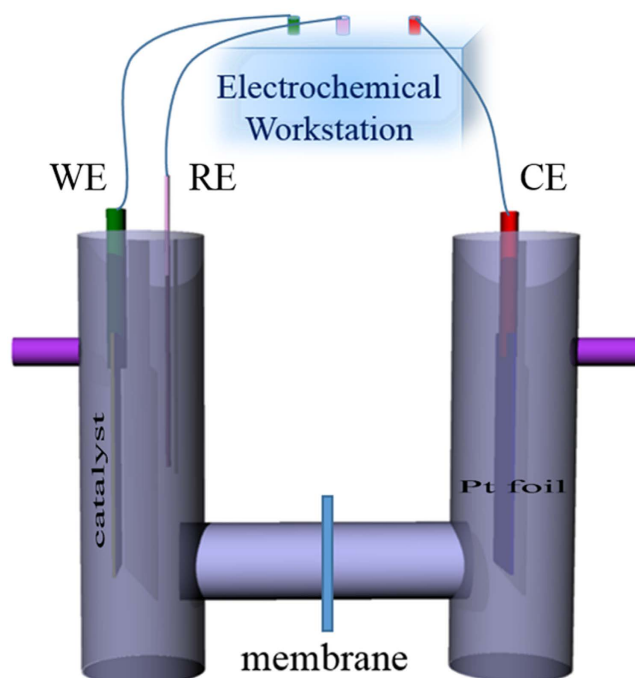
Figure 9. Schematic representation of H₂ production device. Schematic diagram of the home-made gas generation.

X-ray photoelectron spectroscopy (XPS) analysis was performed on a Perkin-Elmer PHI 5000C ESCA system. All binding energies were calibrated by using the contaminant carbon (C1s = 284.8 eV) as a reference.

Electrochemical measurements. Photoelectrochemical measurements were carried out in a conventional three-electrode, single-compartment quartz cell on an electrochemical station (CHI 660D). The H-TiO₂ NTAs electrode and the TiO₂-NTAs electrode with an active area of ca. 4 cm² served as working electrodes. The counter electrode and the reference electrode were a platinum sheet and saturated calomel electrode (SCE), respectively. A bias voltage of 0.7 V was utilized for driving the photo-generated electrons transfer from the working electrode to the platinum electrode. A 300 W Xe lamp with an

ultraviolet filter ($\lambda > 420\,nm$) used as the visible light source was positioned 10 cm away from the photoelectrochemical cell. A 0.5 M Na_2SO_4 aqueous solution was used as the electrolyte. Impedance measurements were performed under illumination (300 W Xe lamp) in 0. 5 M Na_2SO_4 solution at open circuit voltage over a frequency range from 10^5 to 10^{-1} Hz with an AC voltage at 50 mV. The Mott-Schottky plots were obtained at a fixed frequency of 1 KHz to determine the flat-band potential and carrier density.

Hydrogen evolution measurements.   Hydrogen evolution measurements were carried out with a home-made reactor instrument which contains two houses separated by different tubular chambers made by quartz showed in Fig. 9. Such reactor can avoid the mixing of hydrogen generated on the Pt electrode and oxygen (consumed by sanctified agent) generated on the photoanode, and thus the hydrogen and oxygen gases can be separately collected. The home-made reactor device was filled with a 2 M ethylene glycol and 0.5 M Na_2SO_4 solution. Ag/H-TiO_2-NTAs was used as photoanode. SCE electrode was used as reference electrode. Pt foil was used as counter electrode. For testing the amount of the generated H_2, a 0.5 mL of the gas was sampled intermittently through the septum after 1 h visible-light irradiation, and hydrogen was analyzed by gas chromatograph (GC9800 (N)), Shanghai Ke Chuang Chromatograph Instruments Co. Ltd, China, TCD, with nitrogen as a carrier gas and 5 A molecular sieve columns.

References

1. Fujishima, A. & Honda, K. Electrochemical photolysis of water at a semiconductor electrode. *Nature* **238,** 37–38 (1972).
2. El Ruby Mohamed, A. & Rohani, S. Modified TiO_2 nanotube arrays (TNTAs): progressive strategies towards visible light responsive photoanode, a review. *Energy Environ. Sci.* **4,** 1065–1086 (2011).
3. Tahir, A. A., Wijayantha, K. G. U., Saremi-Yarahmadi, S., Mazhar, M. & McKee, V. Nanostructured α-Fe_2O_3 thin films for photoelectrochemical hydrogen generation. *Chem. Mater.* **21,** 3763–3772 (2009).
4. Fu, L., Yu, H., Zhang, C., Shao, Z. & Yi, B. Cobalt phosphate group modified hematite nanorod array as photoanode for efficient solar water splitting. *Electrochem. Acta.* **136,** 363–369 (2014).
5. Jang, Y. H. *et al.* Correction to an unconventional route to high efficiency dye-sensitized solar cells *via* embedding graphitic thin films into TiO_2 nanoparticle photoanode. *Nano Lett.* **12,** 1742–1742 (2012).
6. Li, X. *et al.* Ordered array of gold semishells on TiO_2 spheres: an ultrasensitive and recyclable SERS substrate. *ACS Appl. Mater. Interfaces* **4,** 2180–2185 (2012).
7. Luan, P., Xie, M., Liu, D., Fu, X. & Jing, L. Effective charge separation in the rutile TiO_2 nanorod-coupled α-Fe_2O_3 with exceptionally high visible activities. *Sci. Rep.* **4,** (2014).
8. Wu, W. Q. *et al.* Hydrothermal fabrication of hierarchically anatase TiO_2 nanowire arrays on FTO glass for dye-sensitized solar cells. *Sci. Rep.* **3** (2013).
9. Hesabi, Z. R., Allam, N. K., Dahmen, K., Garmestani, H. & El-Sayed, M. A. Self-Standing crystalline TiO_2 nanotubes/CNTs heterojunction membrane: synthesis and characterization. *ACS Appl. Mater. Interfaces* **3,** 952–955 (2011).
10. Richter, C. & Schmuttenmaer, C. A. Exciton-like trap states limit electron mobility in TiO_2 nanotubes. *Nat. Nano* **5,** 769–772 (2010).
11. Chen, X. & Mao, S. S. Titanium dioxide nanomaterials: synthesis, properties, modifications, and applications. *Chem. Rev.* **107,** 2891–2959 (2007).
12. Singh, M., Salvadó-Estivill, I. & Li Puma, G. Radiation field optimization in photocatalytic monolith reactors for air treatment. *AIChE. J.* **53,** 678–686 (2007).
13. Zhang, Z., Zhang, L., Hedhili, M. N., Zhang, H. & Wang, P. Plasmonic gold nanocrystals coupled with photonic crystal seamlessly on TiO_2 nanotube photoelectrodes for efficient visible light photoelectrochemical water splitting. *Nano Lett.* **13,** 14–20 (2012).
14. Tseng, Y. H., Chang, I. G., Tai, Y. A. & Wu, K. W. Effect of surface plasmon resonance on the photocatalytic activity of Au/TiO_2 under UV/Visible illumination. *J. Nanosci. Nanotechnol.* **12,** 416–422 (2012).
15. Awazu, K. *et al.* A Plasmonic photocatalyst consisting of silver nanoparticles embedded in titanium dioxide. *J. Am. Chem. Soc.* **130,** 1676–1680 (2008).
16. Yamaguchi, T., Kazuma, E.; Sakai, N. & Tatsuma, T. Photoelectrochemical responses from polymer-coated plasmonic copper nanoparticles on TiO_2. *Chem. Lett.* **41,** 1340–1342 (2012).
17. Ye, M., Gong, J., Lai, Y., Lin, C. & Lin, Z. High-efficiency photoelectrocatalytic hydrogen generation enabled by palladium quantum dots-sensitized TiO_2 nanotube arrays. *J. Am. Chem. Soc.* **134,** 15720–15723 (2012).
18. Zhang, N., Liu, S., Fu, X. & Xu, Y. J. Synthesis of M@TiO_2 (M = Au, Pd, Pt) core–shell nanocomposites with tunable photoreactivity. *J. Phys. Chem. C* **115,** 9136–9145 (2011).
19. Jiang, Z., Ouyang, Q., Peng, B., Zhang, Y. & Zan, L. Ag size-dependent visible-light-responsive photoactivity of Ag-TiO_2 nanostructure based on surface plasmon resonance. *J. Mater. Chem. A* **2,** 19861–19866 (2014).
20. Wei, J. *et al.* Ag nanocrystals: 1. effect of ligands on plasmonic properties. *J. Phys. Chem. B* **118,** 14070–14075.
21. Nguyen, N. T., Yoo, J., Altomare, M. & Schmuki, P. "Suspended" Pt nanoparticles over TiO_2 nanotubes for enhanced photocatalytic H_2 evolution. *Chem. Commun.* **50,** 9653–9656 (2014).
22. Choi, H. *et al.* Versatile surface plasmon resonance of carbon-dot-supported silver nanoparticles in polymer optoelectronic devices. *Nat. Photon.* **7,** 732–738 (2013).
23. L. Wu *et al.* Plasmon-induced photoelectrocatalytic activity of Au nanoparticles enhanced TiO_2 nanotube arrays electrodes for environmental remediation. *Appl. Catal. B- Environ.* **164,** 217–224 (2015).
24. Wu, F. *et al.* Photocatalytic activity of Ag/TiO_2 nanotube arrays enhanced by surface plasmon resonance and application in hydrogen evolution by water splitting. *Plasmonics* **8,** 501–508 (2013).
25. Tanahashi, I. Photocatalytic preparation of Ag/TiO_2 films and their localized surface plasmon resonance sensing properties. *B. Chem. Soc. Jpn.* **80,** 2019–2023 (2007).
26. Zhang, Z., Yu, Y. & Wang, P. Hierarchical top-porous/bottom-tubular TiO_2 nanostructures decorated with Pd nanoparticles for efficient photoelectrocatalytic decomposition of synergistic pollutants. *ACS Appl. Mater. Interfaces* **4,** 990–996 (2012).
27. Wang, M. *et al.* P-n Heterojunction photoelectrodes composed of Cu_2O-loaded TiO_2 nanotube arrays with enhanced photoelectrochemical and photoelectrocatalytic activities. *Energy Environ. Sci.* **6,** 1211–1220 (2013).
28. Tachikawa, T. & Majima, T. Exploring the spatial distribution and transport behavior of charge carriers in a single titania nanowire. *J. Am. Chem. Soc.* **131,** 8485–8495 (2009).
29. Kumar, P. M., Badrinarayanan, S. & Sastry, M. Nanocrystalline TiO_2 studied by optical, FTIR and X-ray photoelectron spectroscopy: correlation to presence of surface states. *Thin Solid Films* **358,** 122–130 (2000).

30. Serpone, N., Lawless, D. & Khairutdinov, R. Size effects on the photophysical properties of colloidal anatase TiO_2 particles: size quantization versus direct transitions in this indirect semiconductor? *J. .Phys. Chem.* **99,** 16646–16654 (1995).
31. Lee, H., Lee, Y. K., Hwang, E. & Park, J. Y. Enhanced surface plasmon effect of Ag/TiO_2 nanodiodes on internal photoemission. *J. Phys. Chem. C* **118,** 5650–5656 (2014).
32. Linic, S., Christopher, P. & Ingram, D. B. Plasmonic-metal nanostructures for efficient conversion of solar to chemical energy. *Nat. Mater.* **10,** 911–921 (2011).
33. Clavero, C. Plasmon-induced hot-electron generation at nanoparticle/metal-oxide interfaces for photovoltaic and photocatalytic devices. *Nat. Photon.* **8,** 95–103 (2014).
34. Hu, M. *et al.* Dark-field microscopy studies of single metal nanoparticles: understanding the factors that influence the linewidth of the localized surface plasmon resonance. *J. Mater. Chem.* **18,** 1949–1960 (2008).

Acknowledgments

Author Contributions

Z.L. conceived and designed the experiments. Z.L. and W.W. prepared the samples and performed characterization. Z.L. and G.L. wrote and revised the manuscript. W.W., S.X., X.L., Y.C., D.Z. and H.L helped with the experiment.

Additional Information

Supplementary information accompanies this paper at http://www.nature.com/srep

Competing financial interests: The authors declare no competing financial interests.

How to cite this article: Lian, Z. *et al.* Plasmonic silver quantum dots coupled with hierarchical TiO_2 nanotube arrays photoelectrodes for efficient visible-light photoelectrocatalytic hydrogen evolution. *Sci. Rep.* **5**, 10461; doi: 10.1038/srep10461 (2015).